

Facile preparation and characterization of graphite coated magnetite nanoparticles

V. Rani^{1*}, I. Joshi², P. S. Rawat³ R. C. Srivastava⁴

¹Department of Physics, Sri Ram Singh Dhoni Govt. Degree College, Janti, 263626, Uttarakhand, India

²Department of Chemistry, G.B. Pant University of Agriculture & Technology, Pantnagar, 263145, Uttarakhand, India

³Department of Physics, SALS, Uttaranchal University, Dehradun, 248001, Uttarakhand, India

⁴Department of Physics, G.B. Pant University of Agriculture & Technology, Pantnagar, 263145, Uttarakhand, India

Received: February 22, 2023; Revised: March 13, 2023

A facile procedure for the preparation of graphite coated magnetite nanoparticles with the size of ~ 12 nm using simple chemical co-precipitation method is reported. The co-existence of both phases in the graphite coated magnetite nanoparticles was confirmed by X-ray diffraction. Scanning electron microscopy was used to express its surface morphology. Fourier transform infrared spectroscopy was used to assure the binding of graphite onto the surface of magnetite nanoparticles. Non-isothermal kinetic parameters were calculated by Coats-Redfern method using thermogravimetric analysis curves. DC conductivity was measured by using four probe techniques at room temperature for selected voltage compliances (1V, 10V & 100V). Vibrating sample measurement displayed superparamagnetic behavior with saturation magnetization of graphite coated magnetite nanoparticles was found ~47-54 emu/g. These nanostructures exhibited excellent electrical and magnetic properties which were dependent on the content of the magnetite nanoparticles, making it a promising material for practical applications in biomedical research and nanotechnology.

Keywords: Graphite; Graphite-coated magnetite nanoparticles; Nonisothermal thermodynamics; Hysteresis; DC conductivity

INTRODUCTION

Magnetic nanoparticles have received growing attention over the decades due to their unique properties and applications [1, 2]. These magnetic nanoparticles have tremendous applications in the field of pharmaceuticals, environmental remediation, magnetic resonance imaging, magnetic recording media, data storage, ferro-fluids as well as in various biomedical applications etc. [3-5]. Because of instability and small in particle size, magnetite nanoparticles (MNPs) are difficult to employ for engineering and biomedical applications. MNPs are highly susceptible to oxidant ion when it is exposed to the atmosphere [6]. To overcome this difficulty, several researchers have synthesized magnetic nanoparticles impregnated in a polymer matrix [7]. In addition to inorganic coating, gold [8] and silica [9] with MNPs have been successfully examined as stabilizing shell of magnetic nanoparticles. It was reported that gold shells provide a multifunctional platform for surface modification but it could not protect the magnetic properties due to its grain boundaries. Therefore, new more stable magnetic materials are in demands by industries [10].

Surface functionalization of MNPs is required to improve its physical, chemical and electrical

properties for further applications. The carbonaceous fillers to magnetite matrix provide a remarkable feature to the composites [11]. Carbon based magnetic nanocomposites with accurate their components (matrix and filler material) have unique scientific and technological importance [11]. Graphite (GR) and graphene-oxide (GO) are vastly used as fillers in the composite systems [12,13]. Recently, Meysam *et al.* have prepared carbon/magnetite nanocomposites for copper removal [14]. Malhotra *et al.* [15] modified the magnetic nanoparticles by carbon coating for the increment in bio safety. Magnetite/graphite nanocomposites synthesized and characterized by Kusrini *et al.* [16]. The extraordinary properties of the mentioned fillers have enhanced physical, chemical, mechanical, optical and antimicrobial properties of composite system. [17]. GR has recently attracted considerable attention due to its unique atomic arrangement. It has wide applications in chemical sensors, energy storage, optoelectronics and molecular separation [17-19]. GR nano plates in composite form with magnetic matrices can also enhance the mechanical and corrosion resistance properties [20-22].

Graphitic magnetic nanocomposites are highly demanded due to their extensive applications in

* To whom all correspondence should be sent:
E-mail: vershachauhan31@gmail.com

various fields such as, microwave absorption [23], electro-magnetic shielding [24], water purification [25], adsorption of heavy metal ion and toxic gases from the environment [26, 27], catalysis [28], sensors [29], drug delivery [30-32], and bio-medical diagnosis [33, 34]. In the present work, we have fabricated graphite coated magnetite nanoparticles (GNPs) with different weight ratios using chemical co-precipitation method. The structural, thermal, electrical and magnetic properties of prepared nanostructures were compared with that of GR and MNPs.

EXPERIMENTAL

Starting materials

Graphite powder (500 μM) was procured from Merck (99.98 %), ferrous chloride ($\text{FeCl}_2 \cdot 4\text{H}_2\text{O}$), ferric chloride ($\text{FeCl}_3 \cdot 6\text{H}_2\text{O}$) and ammonia solution were procured from Sd Fine Chemicals India.

Preparation of GNPs

GNPs were prepared through chemical co-precipitation of Fe_3O_4 from a composition of $\text{FeCl}_2 \cdot 4\text{H}_2\text{O}$ and $\text{FeCl}_3 \cdot 6\text{H}_2\text{O}$ in 1:2 molar ratio supplemented with varying weight fractions of GR. The weight fractions of Fe (III) to GR was adjusted to 5:1, 8:1, 15:1 to afford the three samples of GNPs. For the preparation of GNPs involving Fe (III): GR (1:5), a suspension of GR (0.1g/dL, 50 mL) in deionized water was subjected to ultrasonic treatment over 45 min with simultaneous feeding of 50 mL a formulation of Fe (III):Fe (II) in 1:0.6 (w/w, 50 mL) in deionized water @ 0.1 mL/min at 300K. Chemical co-precipitation of Fe_3O_4 in presence of GR was conducted through addition of ammonia solution (30%, v/v) at 85°C till rise in pH level of reaction medium to 10. The contents were allowed for stirring @ 500 rpm over 180 min thereafter cooled to 300K and subsequently centrifuged at ~4000 rpm for 15 min. GNPs settled at the bottom of centrifuge tube were successively washed with deionized water till removal of chloride ions. GNPs were isolated from centrifuge tube through magnetic separation and dried at 400 mmHg/300K. MNPs were also prepared following identical co precipitation method and served as reference for measurement of spectral and electrical, thermal and magnetic properties of GNPs.

Characterization

XRD spectra were recorded on a Bruker D8 Advance spectrophotometer at 30 mA and 40 kV. Average crystallite size (D, nm) were deduced from XRD using Debye Scherrer formula $D = K\lambda/\beta \cos \theta$ using $\text{Cu K}\alpha$ irradiation ($\lambda = 1.54\text{\AA}$) [35-36], where K

is Scherrer constant, β (in radian at full width and half maximum) and θ is the angle of diffraction. Scanning electron measurement (SEM) is used to determine the surface morphology. SEM pictures of synthesized samples were taken for a number of magnifications at FEI QUANTA 200HV. Fourier transform infrared (FTIR) spectra were analyzed over Perkin Elmer spectrophotometer in the wave number (cm^{-1}) ranging in 500-4000. Hysteresis curves were recorded over vibrating sample magnetometer model 155 procured from EG & G Princeton Applied Research, at 300K. DC conductivity (σ_{DC}) measurements were conducted over disk shaped samples with 1.0 cm diameter and 0.1 cm thickness. For this purpose, specimen was fabricated through compression molding at 10 MPa. σ_{DC} data were recorded over Keithley four-point probe arrangement connected with 6221 DC current source and 2182 A nanovoltmeter at 300K. Thermogravimetric curves were recorded over simultaneous thermogravimetric /differential thermal analyzer (TG/DTA) model SII 6300 EXSTAR under progressive heating @ 10°C/ min from ambient temperature to 1000°C in air flow @ 250 mL /min. TG data were used for evaluation of non-isothermal kinetic and thermodynamic parameters of solid state decomposition of GR, MNPs and respective GNPs. Thermal data deduced from TG curve was used for evaluation of activation energy (E_a), pre-exponential factor (A^*), entropy (ΔS), enthalpy (ΔH) and Gibb's free energy (ΔF) pertinent to solid state decomposition using Coats-Redfern equation [37].

$$\log_{10} \left[\frac{-\log_{10}(1-\alpha)}{T^2} \right] = \log_{10} \frac{AR}{\beta E} \left[1 - \frac{2RT}{E} \right] - \frac{E}{2.303RT}$$

where α is the decomposed fraction of material, A^* is pre-exponential factor and R ($\text{J mol}^{-1} \text{K}^{-1}$) is the gas constant. E_a and A^* values are calculated from slope and intercept respectively drawn between $\log [g(\alpha)/T^2]$ against $1000/T$ [Fig. 8].

The change in entropy for activation ΔS ($\text{J K}^{-1} \text{mol}^{-1}$) was calculated according to the relation: $\Delta S = R \ln(Ah/k_B T_s)$, where k_B is the Boltzmann constant, h is the Plank's constant, T_s is the peak temperature deduced from DTA [38, 40].

RESULTS AND DISCUSSION

Microstructure

The surface characteristics of the MNPs and GNPs were found out by using scanning electron microscopy.

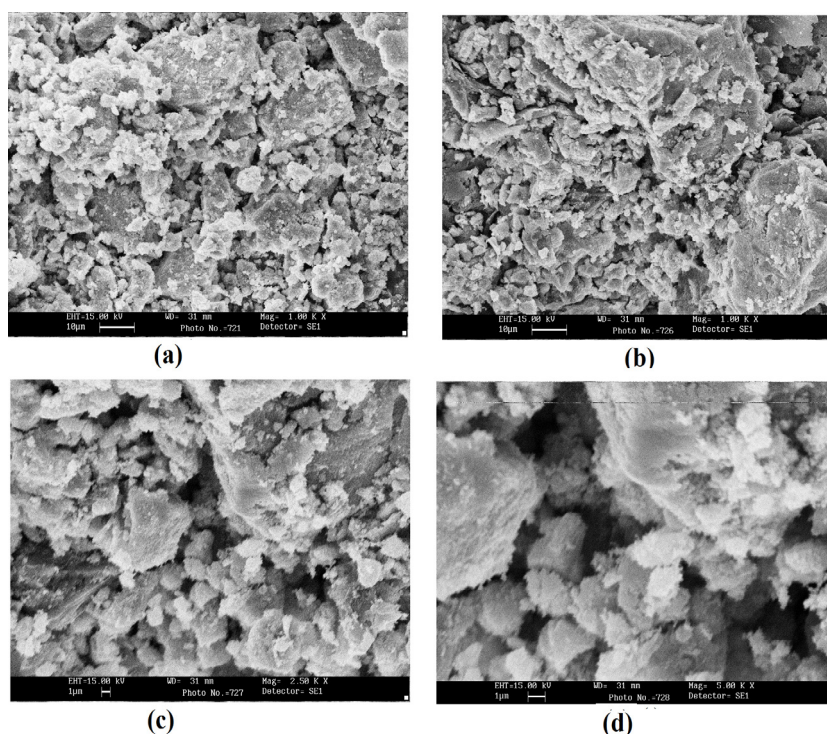


Fig. 1. SEM images for MNPs at 10 μ M, 1 kx (a), for GNPs 10 μ M, 1 Kx (b), 1 μ M, 2.5 Kx (c) 1 μ M, 5 Kx (d)

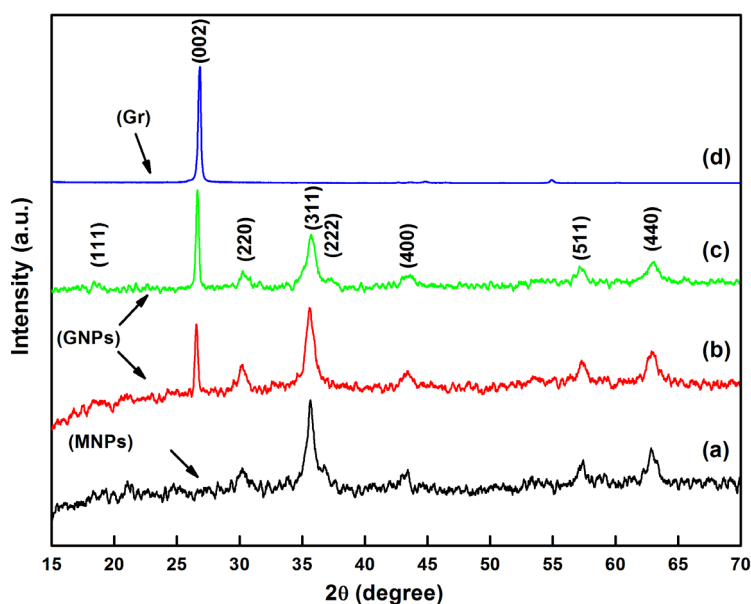


Fig. 2. XRD patterns of (a) MNPs (b) GNPs (I), (c) GNPs (III) and (d) GR.

SEM images (Fig. 1 (a) show that MNPs are spherical in shape with a narrow particle size (17.5 nm which is calculated by the Debye–Scherrer formula). Particles agglomeration is indicating a good connectivity between the grains all together. SEM images of GNPs are shown in fig. 1(b-d). It looks like a smoothed sponge-like structure. XRD measurements reveal the co-existence of phases of MNPs and GR in GNPs. The XRD pattern of the GR [fig.2] shows a sharp peak (002) at $2\theta = 26.81^\circ$ with the interplanar spacing of about 0.33 nm. The absence of any other impurity peak in the XRD of

GR confirms its purity [40-42]. For MNPs, the diffraction peaks at $2\theta = 30.30^\circ, 35.66^\circ, 43.35^\circ, 57.30^\circ, 63.00^\circ$ correspond to (220), (311), (400), (511) and (440) planes respectively. All the diffraction peaks can be identified from the JCPDS card no. 77-1545 [41]. The lattice parameter of MNPs deduced from XRD data was around $\sim 8.36 \text{ \AA}$ which indicates that the product consists of cubic spinel structure and crystalline single-phase of MNPs. In the XRD patterns of the GNPs the expected diffraction peak at $\sim 26.90^\circ$ resulted from GR and remaining peaks can be indexed similar to

MNPs. The similar presence of Graphitic peaks in XRD patterns of Iron oxide can be confirmed by other researches too [44-46]. The average crystallite sizes, as calculated from XRD data using Debye Scherer's formula, was ~17 nm and ~12 nm MNPs and GNPs, respectively.

FTIR spectra

Fig. 3 shows the FTIR spectra of GR, MNPs and as-synthesized GNPs. In the spectrum of GR, the characteristic absorption peaks at ~3447.28 cm^{-1} (ν -O-H) and ~1628.79 cm^{-1} (δ -O-H) attributed the presence of absorbed moisture. It is observed that the peaks in the region about 1520-1600 cm^{-1} assign to the aromatic C=C stretching vibrations and band near 2800-2900 cm^{-1} correspond to the aliphatic carbon [34, 35]. For the spectra of MNPs and GNPs, the band around 586 cm^{-1} is attributed to the stretching vibration (Fe-O) of the tetrahedral groups and band around 445 cm^{-1} is attributed to the octahedral groups [45]. The intense broad band at ~3394 cm^{-1} and the less intense band at 1624 cm^{-1} are due to stretching vibrations corresponding to -OH. Absorption peak around 2356 cm^{-1} attributes to the traces of absorbed CO_2 [48, 49]. The spectra reveals that the C-H and other carbon-based groups are more prominent in MNPs (I) than in MNPs (III) due to high GR content.

Magnetic behavior

Fig. 4 shows the effect of magnetic field on the magnetization (M-H) of MNPs and GNPs. The magnetization was recorded at 300K with the maximum field of 40K Oe.

The samples exhibit immeasurable values of coercive field and remnant magnetization which shows the superparamagnetic nature of all samples [50]. The saturation magnetization of the GNPs (I) and GNPs(III) [~47 emu/g and ~54 emu/g respectively] is smaller than the value of bulk MNPs [~70.5emu/g] [44]. It is observed that saturation magnetization value in GNPs decreases by adding GR into the MNPs [51, 52]. This can be attributed to the small particle size and relatively low amount of MNPs in the GNPs.

DC conductivity

As we know that dc conductivity (σ) measures the ability of substance to conduct electricity [53]. The DC conductivity measurement of samples was investigated under selected voltage compliances (1 V, 10 V, 100 V) at room temperature. The electrical conductivities are shown in Fig 5. As shown in the figure the conductivity of GNPs is much higher than parent MNPs which shows enhanced

semiconducting properties of the synthesized nanostructures.

The DC conductivity of MNPs at 1V shows the value of $\sim 7.45 \times 10^{-4}$ S/cm which increased to the value $\sim 1.38 \times 10^{-3}$ S/cm for highest GR doped GNPs i.e., for GNPs (I). The similar trend was observed for 10V and 100V. This indicates the conductive nature of GR. Among the nanocomposites, GNPs (I) shows highest DC conductivity and the value decreases with further addition of MNPs supported to available literature [54]. The higher conductivity of GNPs(I) may be due to the strong interfacial adhesion between the GR and MNPs.

Thermal behavior

Fig. 6 shows TG thermogram of GR, MNPs and GNPs. As shown in figure, GR renders thermal stability in the range of 25 $^{\circ}\text{C}$ -102 $^{\circ}\text{C}$. Marginal degradation occurs in ~102 $^{\circ}\text{C}$ -570 $^{\circ}\text{C}$ range with the ~1.5% weight loss attributes to moisture content [55]. TG onset for all samples attributes to their low thermo-oxidative stability [56-57, 58]. The decomposition of GR started at 102 $^{\circ}\text{C}$. The first decomposition stage occurs in the range of 570 $^{\circ}\text{C}$ -722 $^{\circ}\text{C}$ associated with weight loss of ~37.4%. The second decomposition stage occurs in the temperature range 742 $^{\circ}\text{C}$ -830 $^{\circ}\text{C}$ with the weight loss of ~56.2% along with DTA signal 79.8 μV at 740 $^{\circ}\text{C}$ [Fig. 7].

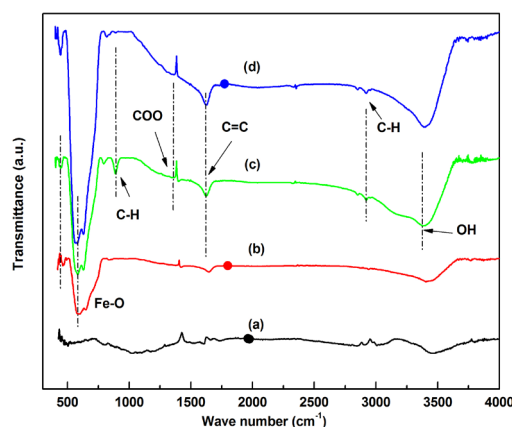


Fig. 3. FTIR spectra of (a) GR, (b) magnetite NPs (c) GNPs (I) and (d) GNPs(III)

Pure MNPs degradation goes in two steps resulting in minor weight loss. The initial weight loss was observed at 102 $^{\circ}\text{C}$ due to the loss of water content. Further slight decrement in the weight is due to the phase change of magnetite (Fe_3O_4) into maghemite (Fe_2O_3) in the temperature range 200 $^{\circ}\text{C}$ -400 $^{\circ}\text{C}$ and afterwards above 420 $^{\circ}\text{C}$, there was no weight loss.

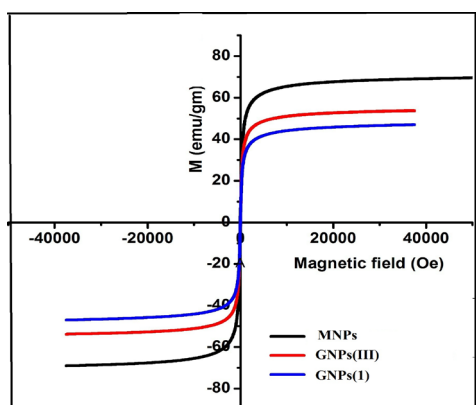


Fig. 4. Magnetization curve (B-H) for ((a) MNPs (b) and (c) GNPs

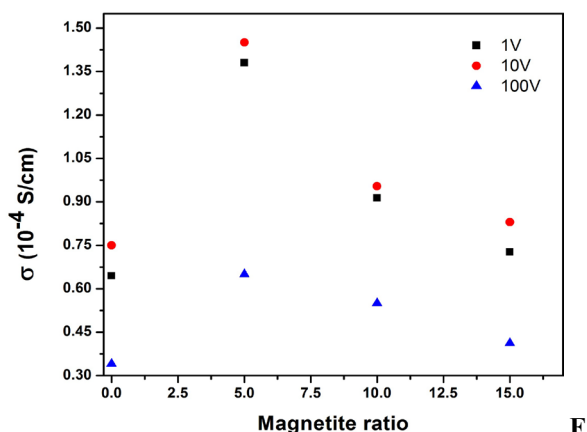
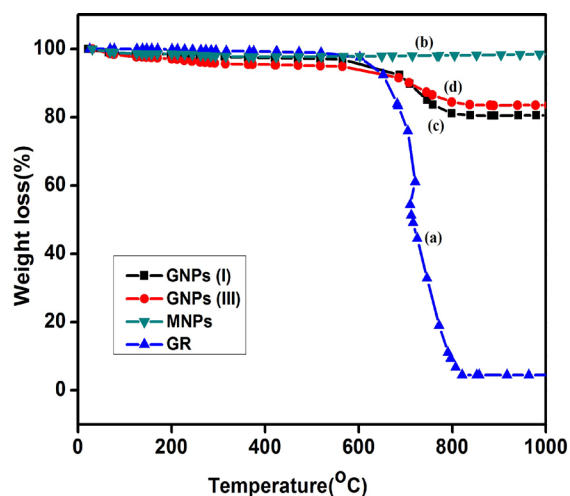


Fig. 5. Electrical conductivities of GNPs at different voltage compliances

GNPs undergo similar degradation as that of GR but with higher thermal stability due to the presence of

relatively thermal resistance MNPs. GNPs (III) thus shows more stability than GNPs(I) [56].

Fig. 6. TG curves for (a) GR, (b) MNPs, (c) GNPs (I)



and (d) GNPs (III).

The results of TGA are in agreement with DTA curves which indicate the exothermic peaks nearly at same temperatures. The determined values of activation energies obtained by CR method can be regarded as indicator of the thermo-oxidative stability of samples. The activation energy for GR was at 157.14 kJ/mol relative to ~159.1 kJ/mol for CNTs [59]. The activation energies for MNPs and GNPs are 22.76 kJ/mol and 129.47 kJ/mol respectively along with negative values of entropy (Table 1).

Table I. Kinetic parameters for solid-state thermal decomposition determined using the Coats–Redfern method.

Samples	T (K)	T _s (K)	E (KJmol ⁻¹)	A (s ⁻¹)	ΔS (KJmol ⁻¹ K ⁻¹)	Parameters	
						ΔH (KJmol ⁻¹)	ΔG×10 ⁵ (KJmol ⁻¹)
GR	844-1100	993	157.14	5.48×10 ⁶	-125.83	149.0	2.72
MNPs	473-673	534	22.76	5.33	-1116.48	18.32	6.14
GNPs(I)	873-1073	987	129.47	2.01×10 ⁵	-153.33	122.43	2.52
GNPs(III)	823-1123	976	98.81	3.92×10 ³	-186.01	106.12	2.89

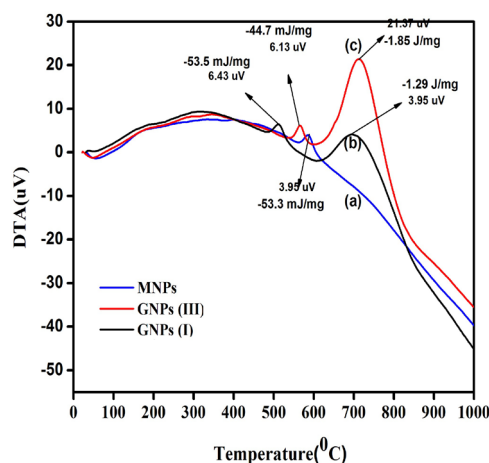


Fig. 7. DTA curves for (a) MNPs (b) and (c) GNPs

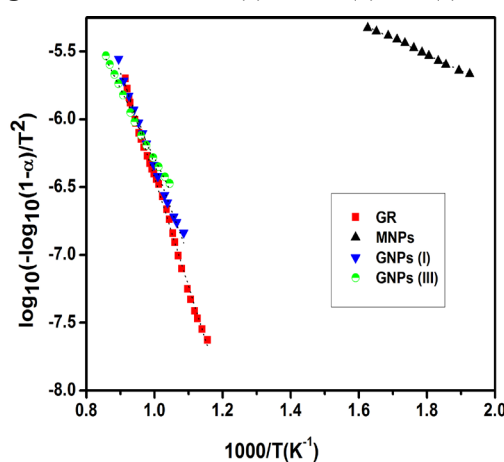


Fig. 8. Coats-Redfern Plots for GR, MNPs and GNPs

CONCLUSION

Graphite coated magnetite nanoparticles with different weight ratios of graphite and magnetite nanoparticles were successfully synthesized by an easy and cost-effective co-precipitation method. The magnetite nanoparticles with the size of ~ 17 nm were attached with graphite layers. The formation of samples were confirmed by XRD and FTIR studies. Graphite coated nanoparticles showed the different thermal, magnetic and electrical properties than their pristine form which defines the wide applicability of such nanostructures. Thermogravimetric analysis reveals that magnetite nanoparticles can improve thermal stability of graphite in synthesized nanostructures. The graphite coated magnetic nanoparticles with superparamagnetic behavior provide the opportunities for various applications in the fields of biomedicine, bio-material separation and bio-diagnostics, etc.

Acknowledgements: Authors would like to acknowledge IIT Roorkee for providing the analytical facilities.

REFERENCES

1. K. A. Abro, I. Khan, J. F. Gomez-Aguilar, *J. Ther. Anal. and Cal.*, **143**(5), 3633 (2021).
2. P. Kulal, V. Badalamoole, *Int. J. Bio. Macromolecules*, **165**, 542 (2020).
3. N. Ahmadpour, M. H. Sayadi, S. Sobhani, M. Hajiani, *J. Env. Management*, **271**, 110964 (2020).
4. T. Muraliganth, A. V. Murugan, A. Manthiram, *Chem. Comm.*, **47**, 7360 (2009).
5. A.C.S. Costa, H.P.A. Alves, M. A. Correa, F. Bohn, W. Acchar. *Mat. Chem. and Phys.*, **232**, 1 (2019).
6. D. Padalia, U. C. Johri, M.G.H. Zaidi, *Physical B, Condensed Matter*, **407**, 838 (2012).
7. T. Agarwal, K. A. Gupta, M. G. H. Zaidi, Sarfraz Alam, *Nanoscience & Nanotechnology*, **2**, (2012).
8. L. León Félix, B. Sanz, V. Sebastián, T. E. Torres, M. H. Sousa, J. A. H. Coaquira, M. R. Ibarra, G. F. Goya. *Scientific Reports.*, **9**, 4185 (2019)
9. X. Ni, Z. Zheng, X. Xiao, L. Huang, L. He, *Mat. Chem. and Phys.*, **120** (1), 206 (2010).
10. A. M. Espinoza-Rivas, M. A. Pérez Guzmán, R. Ortega-Amaya, J. Santoyo-Salazar, C. D. Gutiérrez-Lazos, M. Ortega-López. *J. of Nanotech.*, (2016).
11. S. K. Joshi, A. Kumar, M.G.H. Zaidi, *Defense Sci. J.*, **70**(3), 306 (2020).
12. H. Mudila, P. Parashr, H.L. Kapoor, S. Rana, M.G.H. Zaidi, *Electrochim. Acta*, **38**(2), 69 (2020).
13. S. Mahtab, P. Joshi, B. Arya, M.G.H. Zaidi, T. I. Siddiqui. *M. Sci. Res. India.*, **17** (1), 8 (2020).
14. M. Shahrashoub, S. Bakhtiari, *Mic. and Meso. M.*, **311**, 110692 (2021).
15. N. Malhotra, G. Audira, J. Chen, P. Siregar, H. Hsu, J. Lee, T. Ger, C. D. Hsiao, *Molecules*, **25**(9), 2256 (2020).
16. E. Kusriani, F. Oktavianto, A. Simanjuntak, G. Pasca, A. Usman, *E3S Web of Con.*, **67**, 03029 (2018).
17. H. Mudila, M.G.H. Zaidi, S. Rana, S. Alam, *Carbon let*, **18**, 43 (2016).
18. H. Mudila, M.G.H. Zaidi, S. Rana, V. Joshi, S. Alam. *Int. J. Chem. Anal. Sci.*, **4**(3), 139 (2013).
19. K. Khati, S. Mahtab, M.G.H. Zaidi, I. Joshi, S. Rathore. *Mat. Today.*, **46**(20), 10257 (2020).
20. D. Padalia, U. C. Johri, M.G.H. Zaidi. *Mat. Chem. Phys.*, **169**(89) (2016).
21. B. Wen, X. Zheng. *Composites Sci. and Tech.*, **174**, 68 (2019)
22. A. Jamwal, P. Prakash, D. Kumar, N. Singh, K. K. Sadasivuni, K. Harshit, S. Gupta, P. Gupta. *J of Composite Mat.*, **53**(18), 2545 (2019).
23. X. Huang, J. Zhang, W. Rao, T. Sang, B. Song, C. Wong. *J Alloys and Compounds.*, **662**, 409 (2016).

24. C. K. Madhusudhan, K. Mahendra, B. S. Madhukar, T. E. Somesh, M. Faisal. *Synthetic Metals*, **267**, 116450 (2020)
25. Y. Tian, H. Ma, B. Xing. *Applied Surface Sci.*, **537**, 147995 (2021)
26. R. Foroutan, S. J. Peighambaroust, A. Ahmadi, A. Akbari, S. Farjadfard , B. Ramavandi. *J. of Environ. Chem. Eng.*, **9**(4), 105709 (2021)
27. Y. N. Zhang, Q. Niu, X. Gu, N. Yang, G. Zhao. *Nanoscale.*, **11**(25), 11992 (2019)
28. M. Ahmadi, F. Ghanbari. *Mat. Res. Bulletin.*, **111**, 43 (2019)
29. S. Mehtab, M.G.H. Zaidi, P. Bhatt, P. Joshi, T. Agarwal. *Portugaliae Electrochemica Acta.*, **40**(3), 209 (2022).
30. G. Bisht, M.G.H. Zaidi, S. Rayamajhi. *Int. J of Polymeric Mat. and Polymeric Biomat.*, **66**(14), 708 (2017).
31. G. Bisht, M.G.H. Zaidi. *Drug Delivery and Translational Res.*, **5**, 268 (2015).
32. G. Bisht , M.G.H. Zaidi, *Int. J of Biomedical Material Res.*, **2**(1), 1(2014).
33. C. Xiong, X. Lin, H. Liu, M. Li, B. Li, S. Jiao, W. Zhao, C. Duan, L. Dai, Y. Ni. *J. of the Electrochemical Society*, **166**(16), 3965 (2019).
34. S. Abazari, A. Shamsipur, H. R. Bakhsheshi-Rad, S. Ramakrishna, F. Berto. *Metals.*, **10**(8), 1002 (2020).
35. L. V. Azaroff. McGraw-Hill: New York, NY, USA, 1970.
36. V. S. Vinila, I. Jayakumari. *Micro and Nano Technologies*, 319 (2022).
37. A.W. Coats, J. P. Redfern. *Nature*. **68**, 201(1964).
38. G. Zheng, J.Wu, W. Wang, C. Pan. *Carbon.*, **42**(14), 2839 (2004).
39. V. Rani, R. C. Srivastava, H. M. Agarwal, M.G.H. Zaidi. *Mat. Today: Proc.*, **4** (9), 9471 (2017).
40. P. S. Rawat, R. C. Srivastava, G. Dixit, K. Asokan. *Vacuum.*, **182**, 109700 (2020).
41. Mu Q, Sun Y, Guo A, Yu X, Xu X, Cai A, X. Wang. *Mater Res Express* **6**(9), 950 (2019).
42. R. Madhuvilakku., Y. K. Yen, W. M. Yan, G.W. Huang. *ACS omega*, **7** (18), 15936 (2022).
43. F. Moniriya, S. J. Sabounchei, A. Yousefi, O. Akhavan, *J. Nanoparticle Res.*, **23**(8), 1(2021).
44. J. Sun, L. L.i, R. Yu, X. Ma, S. Jin, K. Chen, Q. Shu. *Molecules*, **25**(13):3044 (2020).
45. C. Li, B. Xie, D. Chen, J. Chen, W. Li , Z.Chen, Y. Long. *Energy.*, **166**, 246(2019).
46. A. T. Ubando, W. H. Chen, H. C. Ong. *Energy*, **180**, 968 (2019).
47. S. M. Fotukian, A. Barati, M. Soleymani, A. M. Alizadeh. *J Alloys and Compounds*, **816**, 152548 (2020).
48. H. Jiang, Y. Cao, F. Zeng, Z. Xie, F. He, *J of Nanomaterials*, 1 (2021)
49. S. Park, C. Raj, J. Manikandan, R. Kim, K. H. Yu. *Bulletin of Korean Chemical Society*, **41** (8), 856 (2020).
50. B. S. Damasceno, A. F. V. da Silva, A. C. V. de Araújo. *J Environmental Chemical Engineering*, **8**(5), 103994 (2020).
51. H. Xiang, G. Ren, Y. Zhong, X. Yang, D. Xu, Z. Zhang, X. Wang. *Mater. Res. Express.*, **8**(2), 025016 (2021).
52. M. S. Raghu, K. Y. Kumar, M. K. Prashanth, B. P. Prasanna, R. Vinut, C. P. Kumar. *J Water Process Engineering*, **17**, 22 (2017).
53. Q. C. Bracamonte, M.Y. Pedram, H. A. Bolados. *Polymers.*, **14**, 4266 (2022)
54. Y. Zhao, L. Liu, J. Han, W. Wu, G. Tong. *J Alloys and Compounds.*, **728**, 100 (2017)
55. M.G.H. Zaidi, D. Sharma, N. Bhullar, V. Agarwal, S. Alam, A. Kumar Rai, R.P. Pant, J. Nanostr. Poly. & Nanocom., **6**(4): 103 (2010).
56. M.G.H. Zaidi, P.L. Sah, S. Alam, A. K. Rai, J. Exp. Nanosci., **4** (1): 55 (2009).
57. P. Joshi, G. Bisht, S. Mehtab, M.G.H. Zaidi. *Materials Today: Proc.*, **62** (12), 6814 (2022)
58. S. Ratkovic, N. Peica, C. Thomsen, D.B Bukur, G. Boskovic .**115**, 1477. (2014).
59. S. Panic, E. Kiss, G. Boskovic. *Reaction Kinetics, Mechanisms and Catalysis.*, **115**, 93 (2015).